Received: 27 September 2019 | Revised: 26 December 2019 | Accepted: 7 January 2020

DOI: 10.1111/ejss.12935

ORIGINAL ARTICLE

European Journal of Soil Science WILEY

Pedogenic information from fine sand: A study in Mediterranean soils

Juan M. Martín-García[1] | **Alberto Molinero-García**[1] | **Julio Calero**[2] | **Manuel Sánchez-Marañón**[1] | **María V. Fernández-González**[1] | **Rafael Delgado**[1]

[1]Departamento de Edafología y Química Agrícola, Universidad de Granada, Granada, Spain

[2]Departamento de Geología, Universidad de Jaén, Jaén, Spain

Correspondence
Alberto Molinero-García, Departamento de Edafología y Química Agrícola, Universidad de Granada, 18071 Granada, Spain.
Email: amolinerogarcia@ugr.es

Funding information
Ministerio de Economía, Industria y Competitividad de España, Grant/Award Number: CGL2016-80308-P

Abstract

The fine sand fraction (50–250 μm) of Mediterranean soils from southern Spain provides valuable information on soil genesis and the origin of their parent materials. This study considers the whole fine sand and heavy fine sand ($\rho > 2.82$ g cm^{-3}) of Luvisols, Calcisols and Fluvisols, which form a chronosequence (ages from 600 to 0.3 ka) of the River Guadalquivir terrace system. Advanced techniques (X-ray diffraction, inductively coupled plasma mass spectrometry, inductively coupled plasma atomic emission spectroscopy, variable pressure scanning electron microscope with an energy dispersive X-ray spectroscopy system and Raman analysis) were employed. Inheritance is the principal pedogenic process. The whole fine sand consisted of carbonates (calcite and dolomite), tectosilicates (quartz, K-feldspar and plagioclases), phyllosilicates (illite/moscovite, biotite, Na-mica, chlorite, kaolinite, interstratified vermiculite-chlorite, vermiculite-illite and smectite-illite) and iron oxides (goethite and haematite). The minor minerals (rutile, anatase, ilmenite, zircon, staurolite, monazite, barite, apatite, andalusite, garnet and titanite) are concentrated, also through inheritance, in the heavy fine sand. However, there is also substantiated evidence for neoformation of rutile in these soils, never reported previously. In addition, we report that (a) the geochemical indices calculated in fine sand (SiO_2/CaO, Chemical Index of Weathering (CIW), Weathering Index of Parker (WIP), Weathering Index (WI), Base Depletion Index (BDI), Weathering Ratio (WR) and Sr/Zr) are closely related to soil age, allowing chronofunctions to be established, and (b) geochemical indices provide information on the origin of soils and permit the establishment of a "critical point" corresponding to "time zero;" that is, the start of pedogenic alteration of the parent material.

Highlights

- Mineralogy and geochemistry inform on the provenance of the fine sand
- Rutile is neoformed in the fine sand and co-exists with the polymorph anatase

- The properties of the fine sand including geochemical indexes fit chronofunctions
- Geochemical indices determine a "critical point" related to the start of weathering

KEYWORDS

geochemical indices, Guadalquivir River, heavy fine sand, Raman spectroscopy, rutile neoformation, soil chronofunction

1 | INTRODUCTION

The sand in soil (granulometric fraction 50–2,000 μm) has been studied in the recent past (20th century) for a variety of reasons, including as a nutrient reserve in tropical soils (Tamm, 1937) or an indicator of the uniformity of the parent material (Arnold, 1968). More recently, it has been used to study specific pedogenic processes such as quartz dissolution (Martín-García, Aranda, Gámiz, Bech, & Delgado, 2004; Martín-García, Márquez, Delgado, Sánchez-Marañón, & Delgado, 2015) and mica alteration (Delgado, Martín-García, Oyonarte, & Delgado, 2003; Martín-García, Delgado, Párraga, Bech, & Delgado, 1998) and as an indicator of the provenance of materials and the degree of alteration in soil chronosequences (Farragallah & Essa, 2011; Sulieman, Ibrahim, Elfaki, & Dafa-Allah, 2015; Tejan-Kella et al., 1991). Nonetheless, relatively few studies have employed the sand in soils to investigate pedogenesis, and there are even fewer studies in Mediterranean soils. This may be due to sand only being considered useful, historically, for providing information on parent material type and its degree of alteration, because it is assumed to be inherited from the parent material. By contrast, the sand fraction is frequently studied in sedimentology. For example, Hernández-Hinojosa, Montiel-García, Armstrong-Altrin, Nagarajan, and Kasper-Zubillaga (2018) analysed the mineralogy of sands along the Western Gulf of Mexico using X-Ray diffraction (XRD) and scanning electron microscopy–energy dispersive X-ray spectroscopy (SEM–EDX) and their geochemistry by X-ray fluorescence, to evaluate the intensity of chemical weathering, provenance and tectonic environment.

The use of geochemical indices of evolution/alteration is another method employed in the study of the sand fraction (Garzanti & Resentini, 2016; Liu, Jin, Sun, & Zhao, 2016). These indices generally consider the mobile chemical elements (mainly alkaline and alkaline earth metals) in relation to the least mobile elements (principally silica (Si), aluminium (Al) and iron (Fe)). The indices are primarily conditioned by the minerals containing these elements and the resistance of these minerals to alteration. Geochemical indices have been employed in soils to estimate the degree of evolution (Schaetzl & Thompson, 2015) because, during pedogenesis, unstable minerals are eliminated faster than those that are resistant. These indices are also useful in studies on the provenance of materials (Garzanti & Resentini, 2016); nonetheless, there is a notable absence of soil studies with these objectives, particularly involving the sand fraction.

A soil chronosequence is a series of soils which differ in their profile development due to their differences in age, whereas the other soil-forming factors remain constant if possible. In the basin of the River Guadalquivir (the most important fluvial system in the southern Iberian Peninsula), a system of four fluvial terraces and a floodplain constitute an almost ideal soil chronosequence: Calero, Delgado, Delgado, and Martín-García (2008) found that Harden's Profile Development Index (PDI) and some important soil analytical properties of the fine earth fraction (<2 mm), and field morphological characteristics of soil quantified by optimal scaling, fit significant chronofunction equations; furthermore, some fabric morphometric attributes measured by scanning electron microscopy image-analysis (SEM-IA) also fit chronofunctions (Calero, Delgado, Delgado, & Martín-García, 2009). The transmission electron microscopy with analytical electron microscopy (TEM-AEM) and XRD studies of mica and smectite in silt (2–50 μm) and clay (<2 μm) fractions (Calero, Martín-García, Delgado, Aranda, & Delgado, 2013) permitted determination, at the nanoscale level, of statistically significant logarithmic chronofunctions of the crystallochemical parameters; Martín-García et al. (2016) studied some mineralogical (XRD), crystallochemical differential X-ray diffraction (DXRD), geochemical inductively coupled plasma mass spectrometry (ICP-ms) and inductively coupled plasma atomic emission spectroscopy (ICP-AES) and diffuse reflectance spectroscopy (DRS) colour parameters of the clay fraction of these soils, most of which showed logarithmic chronofunctions with asymptotes at 70–100 ka; and finally, Martín-García et al. (2019) established chronofunctions with the contents of lanthanides. However, the role of fine sand in this chronosequence has not been studied.

Consequently, the aim of the present research, centred on the Mediterranean soils from the River Guadalquivir chronosequence, was to investigate the

chemical and mineralogical compositions and morphology at the SEM scale of the soil fine sand fraction. The evolution/alteration indices of fine sand were calculated. An original aspect of this study is the investigation of chronofunctions with the properties measured in the fine sand. All of this is in order to elucidate the pedogenetic applications of fine sand. These themes have scarcely been studied to date.

2 | MATERIALS AND METHODS

2.1 | Setting and soils

The alluvium of the River Guadalquivir (Figure 1a) consists of gravels with some stone-free sandy or silty layers derived from lithologically diverse rocks in the drainage basin: igneous rocks (acids, alkaline and intrusive rocks) and metamorphic rocks from the Iberian Massif (Carracedo, Larrea, Alonso-Olazabal, & Gil-Ibarguchi, 1997; Larrea et al., 1992; Larrea, Carracedo, Ortega, & Gil-Ibarguchi, 1994, 1995; Larrea, Carracedo, Yusta, Ortega, & Gil-Ibarguchi, 1996; Martínez et al., 2008; Pascual, Donaire, & Pin, 2008; Pin, Liñán, Pascual, Donaire, & Valenzuela, 2002); sedimentary rocks from the External Betic Zones of the Betic Cordilleras (Martínez-Ruiz, 1994; Ortega-Huertas, Palomo, Moresi, & Oddone, 1991); metasedimentary rocks from the Internal Betic Zones of the Betic Cordilleras (Torres-Ruiz, Pesquera, Gil-Crespo, & Velilla, 2003); and quaternary sediments from the Guadalquivir Depression–Cenozoic Basin (Jiménez-Espinosa, Jiménez-Millán, & García-Tortosa, 2016; Martínez et al., 2008).

The study area is located between the towns of Andújar and Villanueva de la Reina (Figure 1b) in the middle reaches of the Guadalquivir River. Five representative soil profiles (P1 to P5) were selected from a post-incisive soil chronosequence on fluvial terraces of the Guadalquivir River (Terrace 1 to Terrace 4 and Flood Plain) (Figure 1b; Table 1). The ages of the surfaces range from 600 to 0.3 ka. Preholocenic terraces are Terrace 1 (600 ka), Terrace 2 (300 ka) and Terrace 3 (70 ka). Holocenic surfaces are Terrace 4 (7 ka) and the Flood Plain (0.3 ka). The soil surface ages were determined by Santos-García (1988), Santos-García, Jerez-Mir, and Saint-Aubin (1991) and Carral, Martín-Serrano, Sansteban, Guerra, and Jiménez-Ballesta (1998). Together with the soil profiles, fresh point bar sediments of the Guadalquivir River course were also sampled. The climate is Mediterranean (mean annual temperature of 18°C and total annual precipitation of 650 mm). Currently, the soils are mainly used for the cultivation of olives and other crops (mainly wheat and cotton).

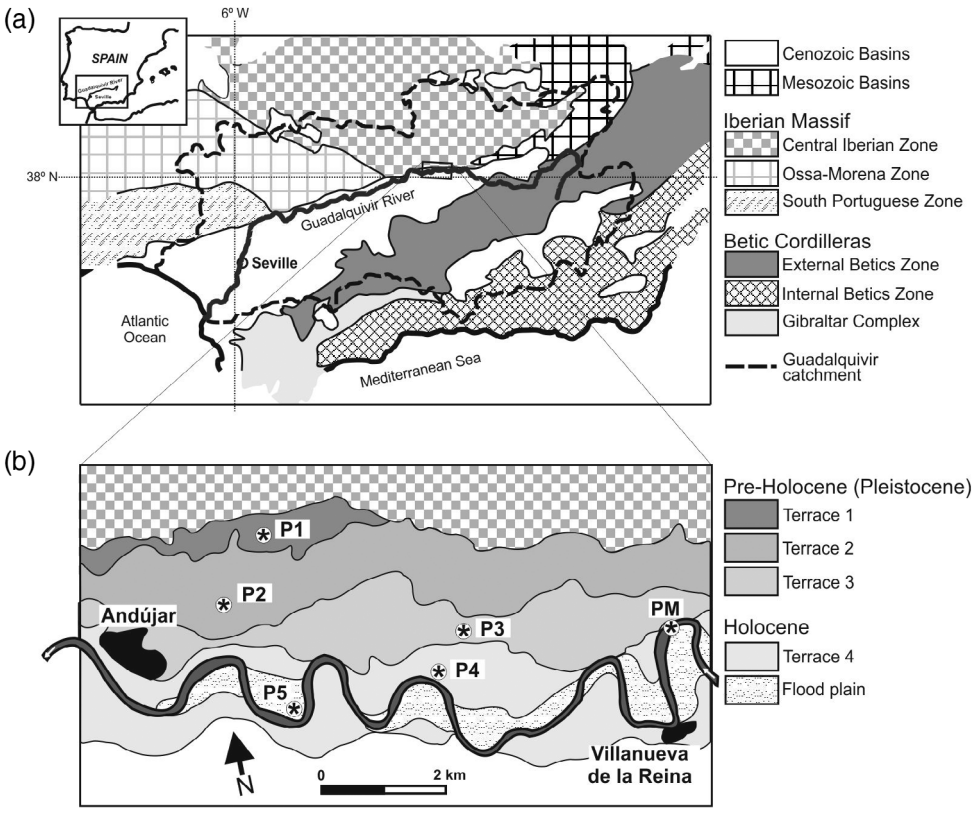

FIGURE 1 Study area: (a) location and geology of the Guadalquivir catchment; (b) position of fluvial terrace levels and soil sampling

2.2 | Samples and soil fine sand analyses

The bulk soil samples were air dried and sieved to <2 mm to obtain the fine earth. Subsequently, and after the removal of organic matter with H_2O_2, the fine sand fraction (50–250 μm) was separated by wet sieving and collected on quartered aliquots for later analysis (these samples are denoted as "whole fine sand" in this study). For some analyses (such as the XRD study and variable pressure scanning electron microscope (VP-SEM) observations), the whole fine sand fraction was separated gravimetrically with bromoform ($\rho = 2.82\ g\ cm^{-3}$) in order to concentrate the heavy fraction, denoted as "heavy fine sand."

The quantitative mineralogical composition of whole fine sand was determined by XRD (powder method) with a Siemens D5000 X-ray diffractometer (Siemens, Karlsruhe, Germany) under the following conditions: Cu *Kα* radiation, 35 kV, 15 mA and a step size of 0.05 °2θ. Mineral percentages were estimated by the intensity factor method (Martín-García, Delgado, Sánchez-Marañón, Párraga, & Delgado, 1997). For selected heavy fine sand samples, a qualitative study was carried out using XRD (same apparatus and conditions).

Selected samples of whole fine sand were examined morphologically and analytically using a VP-SEM, Zeiss SUPRA40VP equipment (Carl Zeiss SMT GmbH, Oberkochen, Germany), acceleration voltage at between 0.2 and 30 kV, in conventional mode, with a backscattered electron detector (AsB images), equipped with an EDX detector, and with a structural and chemical analyser by Raman spectroscopy inside the measurement chamber of the SEM (SCA-Raman), with two laser excitation lines at 532 and 785 nm. The samples were mounted on aluminium sample holders on double-sided adhesive carbon paper and metallized with carbon. The use of the VP-SEM in backscattered electron images mode permitted

TABLE 1 Characteristics of the soil chronosequence sampled in the Guadalquivir river terraces (SE Spain)[a]

Chronosequence level	P1	P2	P3	P4	P5	PM
Altitude/m	250	230	215	206	200	200
Age/ka	600, pre-Holocene	300, pre-Holocene	70, pre-Holocene	7, Holocene	0.3, Holocene	0.001,
Holocene Soil[b]	Cutanic Luvisol	Lixic Calcisol	Cutanic Luvisol	Haplic Calcisol	Haplic Fluvisol	Alluvial[c]
Horizons (HDI[d])	Ap (0.38), Bt (0.52), Btg1 (0.44), Btg2 (0.44), 2BCtg (0.33), 3BCt (0.33), 4C (0.19)	Ap (0.44), Btg1 (0.52), Btg2 (0.54), Btk (0.51), Cmk/Btk (0.35)	Ap1 (0.31), Ap2 (0.28), Bt1 (0.45), Bt2 (0.46), Bt3 (0.58), Bt4 (0.56), Bt5 (0.48), 2Bt6 (0.35), 3Bt7 (0.33)	Ap1 (0.37), Ap2 (0.31), Bwk1 (0.33), 2Bwk2 (0.35), 3C1 (0.16), 4C2 (0.09)	Ap (0.28), 2C1 (0.16), 3C2 (0.09), 4C3 (0.20), 5C4 (0.10), 6C5 (0.17), 7C6 (0.19)	Point-bar deposit (0.00)
PDI[d]	44.8	44.3	39.6	26.8	21.2	0
Solum thickness/m	1.65	>0.89	1.83	0.75	0.32	
Moist colour[e] (Munsell)	6.4YR 4.2/5.5	5.6YR 4.8/6.0	5.6YR 3.9/5.6	9.2YR 4.2/3.5	10YR 4/3	2.5Y 5/3
Clay[e]/%	32.3	42.4	31.3	29.7	23.0	16.3
Fine sand[e]/%	31.9	20.6	33.5	31.0	41.5	21.6
Organic C[e]/%	0.24	0.35	0.21	0.48	0.77	1.76
Carbonates[e]/%	0.8	16.2	0.0	26.0	38.4	23.5
pH[e]	7.3	7.9	7.6	8.1	7.9	8.4
CEC[e]/$cmol_+kg^{-1}$	8.9	14.4	10.5	11.3	12.8	8.7

[a]Data summarized from Calero et al. (2008, 2009, 2013) and Martín-García et al. (2016).
[b]Soil classification (IUSS Working Group WRB).
[c]Current sediments.
[d]HDI, Horizon Development Index; PDI, Profile Development Index (Martín-García et al., 2016).
[e]Mean values of solum or sediment, measured in fine earth (<2 mm).
Abbreviation: PM, point-bar sediments.

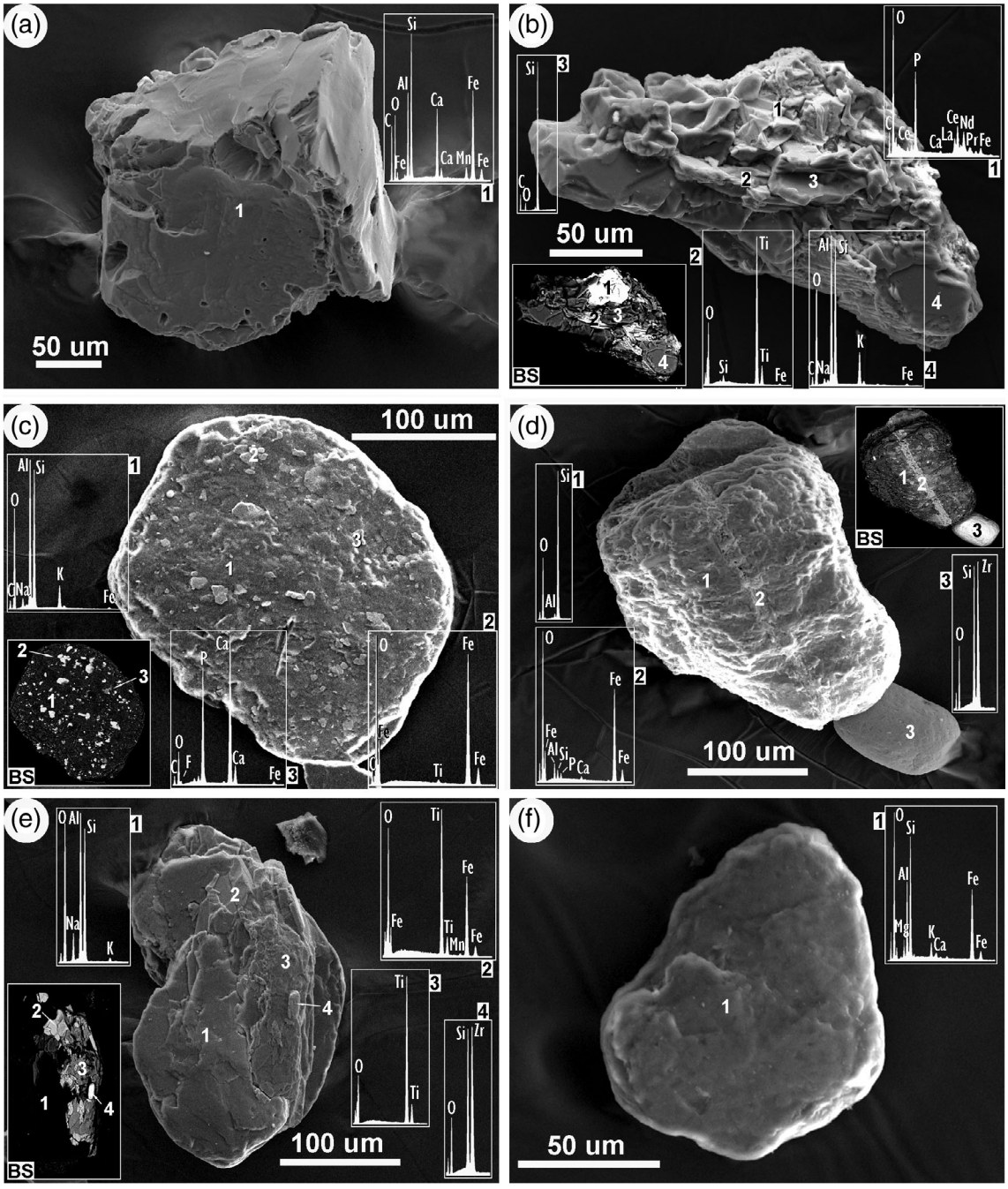

FIGURE 2 Conventional and backscattered (BS) variable pressure scanning electron microscope (VP-SEM) images and energy dispersive X-ray (EDX) microanalysis of fine sand-sized mineral grains. (a) Profile P4, horizon 4C2: monomineral grain of garnet (nesosilicate, variety andradite). (b) Profile P5, horizon 6C5: polymineral grain of monazite (1), titanium oxide (Tiox) (2), quartz (3) and K-mica (muscovite or illite) (4). (c) Profile P5, horizon 6C5: monomineral grain of K-mica (muscovite or illite) (1), although with iron oxides adhering to surface (2) (goethite and/or haematite) and apatite (3). (d) Profile P1, horizon 2BCtg: polymineral grain of quartz (1) with fissure filled with iron oxides (goethite and/or haematite) and apatite (2). Monomineral grain of zircon (3) of exceptional size (>100 μm), sub-rounded and polished by fluvial activity. (e) Profile P5, horizon 6C5: polymineral grain consisting of plagioclase (1) (probably albite), ilmenite (2), titanium oxide (Tiox) (3) and zircon (4). (f) Profile P3, horizon Bt2: monomineral grain of K-mica (biotite). (g) Profile P1, horizon 2BCtg: monomineral grain of barite. (h) Profile P2, horizon Btg2: polymineral grain of K-mica (muscovite or illite) (1) and monazite (2). (i) Profile P4, horizon 4C2: grain of dolomite. (j) Profile P4, horizon 4C2: polymineral grain composed of titanium oxide (Tiox) (1), staurolite (prism face {110} and pinacoid face {010}) (2) and quartz (3). (k) Profile P1, horizon 2BCtg: monomineral grain of titanite. (l) Profile P5, horizon 6C5: tabular polymineral grain, consisting mainly of ilmenite (1) with a plagioclase inclusion (albite) (2)

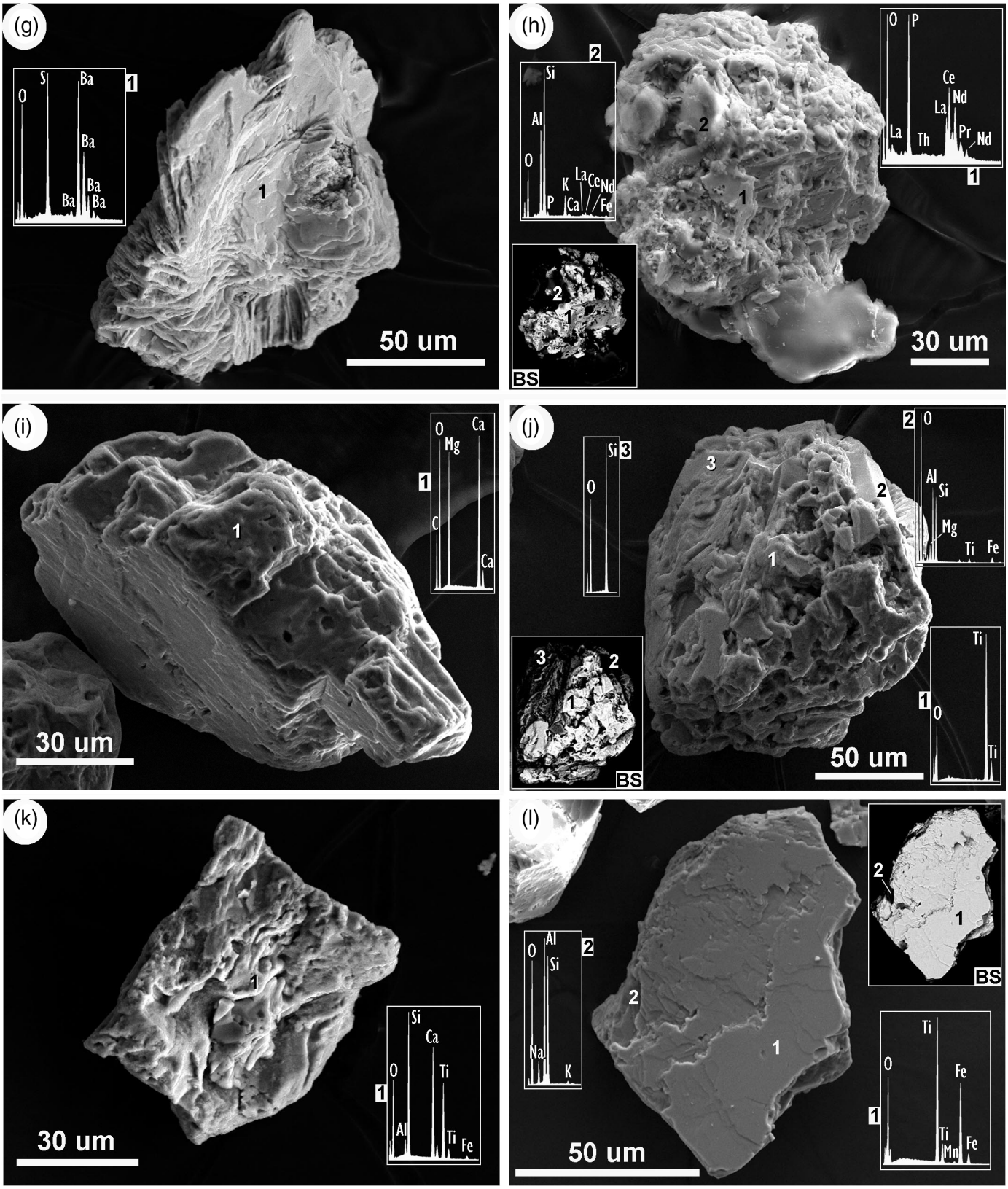

FIGURE 2 (Continued)

the detection of minerals with elements of relatively high atomic mass, due to its greater luminosity. In the case of TiO_2 polymorphs, SCA-Raman allowed differentiation of rutile crystals (space group: $P4_2/mnm$) from those of anatase (space group: $I4_1/amd$). In the VP-SEM studies, at least 50 grains per sample were analysed.

Chemical analyses of whole fine sand were carried out at the Natural History Museum laboratories (London, UK). Following a lithium metaborate fusion and nitric acid digestion, the following were determined: (a) major oxides, by ICP-AES: SiO_2, Al_2O_3, CaO, Fe_2O_3, K_2O, MgO, Na_2O, P_2O_5 and TiO_2; (b) trace elements, by ICPms: Sc, V, Cr, Mn, Co, Ni, Cu, Zn, Ga, Rb, Sr, Y, Zr, Nb, Mo, Sn, Cs, Ba, Hf, Ta, W, Tl, Pb, Th and U. The sum of the lanthanide elements (ΣREE) was taken from Martín-García et al. (2019). Several weathering indices were used to estimate the extent of chemical alteration:

SiO_2/CaO;

Chemical Index of Weathering (CIW) (Harnois, 1988): $CIW = 100 \times Al_2O_3/(Al_2O_3 + CaO + Na_2O)$;

Weathering Index of Parker (WIP) (Parker, 1970): $WIP = 100 \times (CaO_{MOLAR}/0.7 + MgO_{MOLAR}/0.9 + 2Na_2O_{MOLAR}/0.35 + 2K_2O_{MOLAR}/0.25)$;

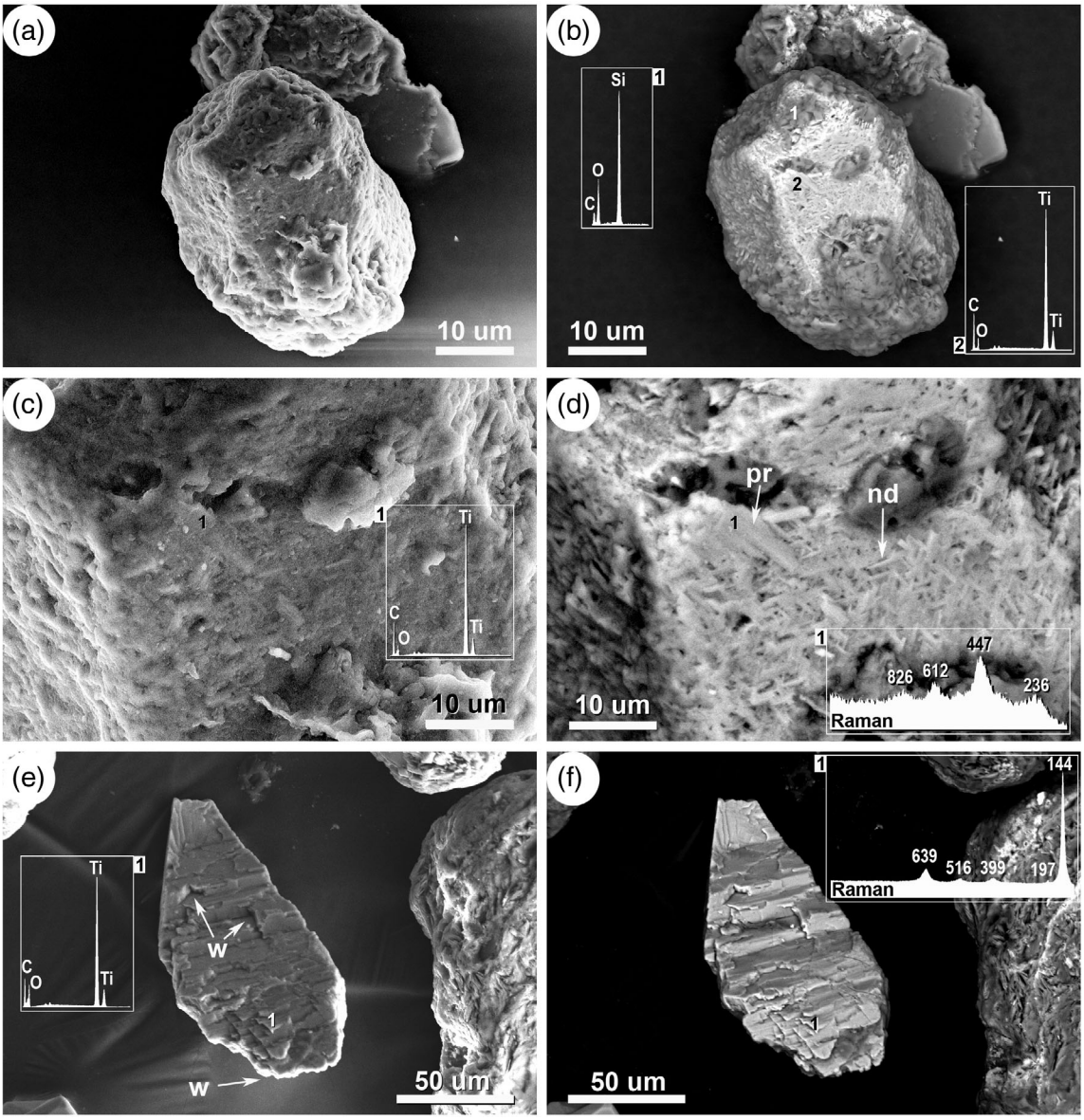

FIGURE 3 Variable pressure scanning electron microscope (VP-SEM) images with energy dispersive X-ray (EDX) and Raman spectra of the whole fine sand of horizon 2BCtg (P1). (a), (c) and (e) are in conventional mode; (b), (d) and (f) in backscattered mode. (a) and (b): mineral grain of quartz (SiO_2) with "coating" of rutile (TiO_2) on one of its faces, visible in b as a light grey colour. (c) and (d): detail of (a) and (b) of rutile coating. (c) Shows TiO_2 composition by EDX spectrum. In (d) the Raman spectrum confirms the presence of rutile and also shows the presence of rutile in a fabric, often interwoven, of acicular crystals (nd) of 3 × 0.5 μm (approx.) with some larger prismatic crystals (pr) of 10 × 2 μm. (e) and (f): grain of anatase. In (e), the EDX spectrum shows composition of TiO_2, whereas in (f), the Raman spectrum confirms the anatase and that the grain is weathered (w) physically and chemically

Weathering Index (WI) (Vogel, 1975): $WI = 100 \times (CaO + MgO + Na_2O + K_2O)/(SiO_2 + Al_2O_3 + Fe_2O_3 + CaO + MgO + Na_2O + K_2O)$;

Base Depletion Index (BDI) (Jien, Baillie, Huang, Chen, & Chiu, 2016): $BDI = (CaO + MgO + Na_2O + K_2O)/(Al_2O_3 + Fe_2O_3 + TiO_2)$;

Weathering Ratio (WR) (Chittleborough, 1991): $WR = (CaO + MgO + Na_2O)/ZrO_2$; and

Sr/Zr (Muhs, Bettis, Been, & McGeehin, 2001).

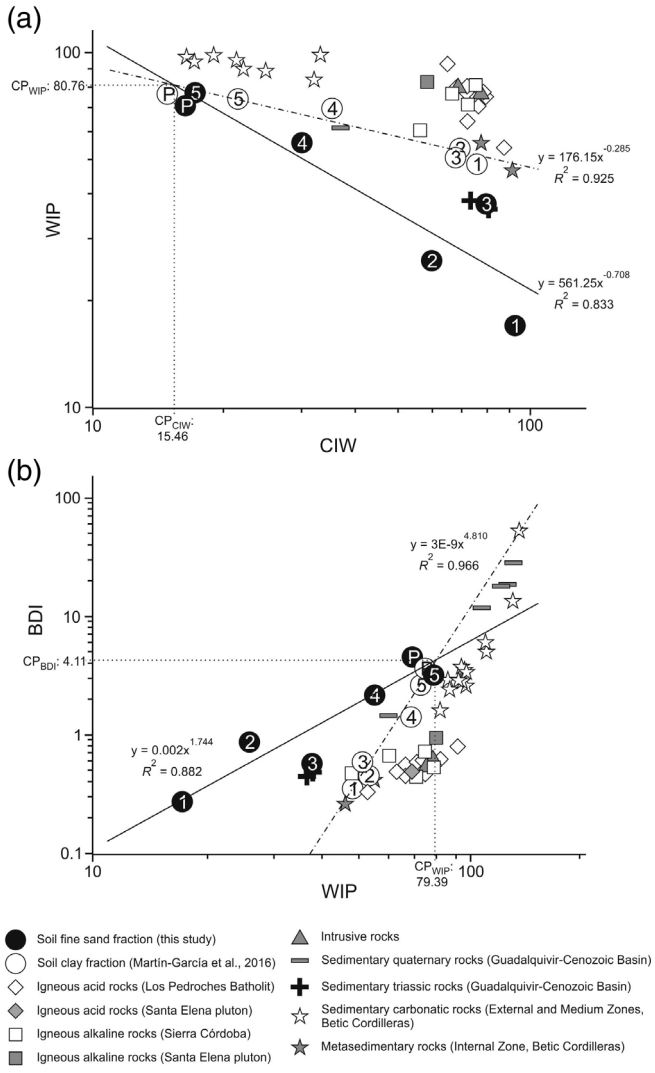

FIGURE 4 Relationships between geochemical indices CIW (Chemical Index of Weathering) and WIP (Weathering Index of Parker) (a) and WPI and BDI (Base Depletion Index) (b) for soil whole fine sand and soil clay fractions (mean profile values) (Table 2). They include the values for rocks from the Guadalquivir catchment (igneous, sedimentary and metasedimentary). The numbers in the circles correspond to soil profiles, and P to point bar sediments. The lines (and adjacent equations) correspond to the straight lines of correlation for the population of samples of soil fine sand (continuous) and soil clay (dots and dashes) fractions. CP indicates the values of the indices at critical intersection points

Some of these weathering indices were calculated for the clay fraction of these soils by using Martín-García et al.'s (2016) data.

Statistical analysis was carried out using the IBM SPSS v.22.0 software package.

3 | RESULTS

3.1 | XRD mineralogy

The following minerals were identified in the whole fine sand (Table S1): the phyllosilicates K-mica, Na-mica (paragonite), chlorite, kaolinite, and some 2:1 phyllosilicate phases with spacings between 1.23–1.53 and 1.0–1.22 nm (identified by Calero et al. 2013 as smectite, chlorite and interstratified vermiculite-chlorite, vermiculite-illite and smectite-illite), tectosilicates quartz and feldspars (K-feldspar and plagioclases), iron (hydr)oxides (goethite and haematite) and carbonates (calcite and dolomite).

The XRD mineralogy of the heavy fine sand fraction of selected samples (Table S1, Figure S1; supported by Figures 2 and 3) revealed a range of mineral classes (and species): oxides (rutile, anatase, ilmenite, goethite and haematite), silicates (zircon, staurolite, quartz, K-mica, andalusite, garnet, chlorite and titanite) and carbonates (calcite and dolomite). This composition (Table S1) is different to that of the whole fine sand, although with a few coinciding mineral species: quartz, K-mica, chlorite, goethite, haematite, calcite and dolomite. The presence of light minerals in the heavy fine sand (Table S1, Figure S1), with densities close to or lower than that of bromoform, 2.82 g cm^{-3} (quartz, calcite, K-mica and chlorite), can be explained by: (a) the polymineral nature of many of the grains (Figure 2b–e,h,j,l), both heavy and light; (b) the presence of coverings of heavier minerals on the grains (e.g., iron oxides; Figure 2c); and (c) possible small differences in mineral composition (which change it to "heavy") that were undetectable with the techniques used in this study.

3.2 | VP-SEM–EDX mineralogy of the whole fine sand

The VP-SEM–EDX images (Figure 2) have proved highly informative due to the following. (a) The mineralogy is confirmed for some of the major phases identified with XRD (Table S1): quartz, calcite, dolomite, K-feldspar and chlorite. (b) The mineral species of some of the phases identified with XRD are established: K-mica is both biotite (Figure 2f,i) and muscovite-illite (Figure 2b,c,h,i); plagioclase is predominantly albite type (Na-plagioclase) (Figure 2e,l). (c) The mineralogical inventory is

completed with minor species (mainly heavy minerals), which are difficult to detect with XRD due to their low contents. The presence of heavy atoms in the mineral composition is frequently shown in the backscattered electron images (BS in Figure 2) by bright tones close to white. The following minority species were detected: garnet (nesosilicate, variety andradite) —$Ca_3Fe_2(SiO_4)_3$— (Figure 2a), monazite —(Ce,La,Nd,Pr)PO_4— (Figure 2b,h), titanium oxide-rutile or anatase, TiO_2— (Figure 2b,e,j), apatite —$Ca_5(PO_4)_3(OH)$— (Figure 2c,d), zircon —$ZrSiO_4$— (Figure 2d,e), ilmenite —$FeTiO_3$— (Figure 2e,l), barite —$BaSO_4$— (Figure 2g), staurolite —$(Fe,Mg)_2Al_9(Si,Al)_4O_{20}(O,OH)_4$— (Figure 2j) and titanite —$CaTiSiO_5$— (Figure 2k). Iron oxides were also found in many of the grains (Figure 2c,d). Although VP-SEM–EDX does not permit mineral species identification, these were either goethite or haematite. The same occurred with the TiO_2 polymorphs, rutile and anatase. However, it was possible to identify these species of Fe and Ti using XRD (Figure S1). (d) Consideration of the mineralogical results derived from Figure 2 together with the XRD results (Table S1, Figure S1) confirms that the fine sand (both whole fine sand and heavy fine sand) is a complex of at least 25 different mineral species (20 in horizon 4C2 of P4 alone).

Another finding that confirms the usefulness of VP-SEM–EDX is the proof that many of the fine sand grains are polymineral (Figures 2b–e,h,j,l and 4a), although some are monomineral (Figures 2a,f,g,i,k and 3e).

3.3 | VP-SEM–EDX-Raman study of TiO_2 polymorphs in fine sand

Rutile and anatase (polymorphs of titanium dioxide) were found together in the soils using XRD (Table S1, Figure S1). Using VP-SEM–EDX, the presence of TiO_2 was described (Figure 2a,e,j) without being able to distinguish the grains of the two species, as this is not possible with EDX. Consequently, Raman spectroscopy was used (Figure 3d,f). Rutile showed maxima at 143, 236, 447, 612 and 826 cm^{-1} and anatase at 144, 197, 399, 516 and 639 cm^{-1} (Arsov, Kormann, & Plieth, 1991). Rutile, more abundant than anatase, was found in polymineral or even monomineral grains, comprised of prismatic crystals. Rutile was also observed (Figure 3a–d) covering the faces of quartz grains as micrometric acicular and prismatic crystals, which appear to result from pedogenic recrystallization *in situ* (authigenic) of a colloid/gel of TiO_2. Two further observations are of interest: the tendency of the acicular and prismatic crystals to cross (Figure 3d), following the typical rutile-law twin (twinning on {011}), and that the crystal support is quartz (Figure 3b) due to the well-known quartz-rutile association (Klein & Dutrow, 2007).

3.4 | Major and minor chemical elements

The content of SiO_2 varied between 51.68 and 90.36% (Table S2) and was more abundant in pre-Holocene soils (P1, P2 and P3) than in Holocene soils (P4 and P5) and point bar sediments. The content of CaO ranged from 0.06 to 23.60%, decreasing dramatically in the pre-Holocene soils.

Minor elements (Table S3) exhibited variability between the different soils and terraces. Cr, Mn, Ni, Rb, Sr, Zr, Ba and ΣREE were the only elements to exceed 100 mg kg^{-1} in at least one sample (Cr and Ni only in Btg2 of P2, where their contents easily exceeded those of the other horizons). The concentrations (means per profile) of some minor elements such as Mn, Sr, Cs, Hf and W showed dependence on the age groups of the soils (pre-Holocene vs. Holocene): Cs, Hf and W were more abundant in pre-Holocene soils; Mn and Sr were more abundant in Holocene soils. The maximum value of Zr (mean per profile) was that of P1.

4 | DISCUSSION

4.1 | Mineralogy of fine sand

Quartz was the principal component in all horizons of the oldest soils, that is, pre-Holocene P1, P2 and P3 (between 47 and 78%) (Table S1), so it can be assumed to be a resistant phase that is concentrated by inheritance during pedogenesis. In the most recent soils, that is, Holocene-P4 and P5, the carbonates (calcite + dolomite) were the most abundant (>38%) in most of the horizons. However, in 2Bwk2 of P4 they accounted for only 1%, due to lithological discontinuity. Consequently, quartz and carbonate (calcite + dolomite) contents depend on soil age and, as major components of these fine sands, their percentages are inversely related ($R^2 = 0.866$; $n = 24$).

The pronounced changes in XRD mineralogy (Table S1) confirm the presence of some of the lithological discontinuities already established morphologically and/or granulometrically. Of particular interest are those in horizons 2Bwk2 of P4, 2BCtg of P1 (with an increase in quartz and a decrease in K-feldspars) and 4C3 of P5 (with an increase in total phyllosilicates). In none of these examples can the mineralogical changes be explained by the action of pedogenic processes within the soil.

The dominant formation process of minerals from the heavy fine sand (Table S1) must be inheritance, because the majority are detrital species and thus originate from the geological materials of the zone. However, there are also other genetic possibilities (see section "VP-SEM–EDX-Raman study of TiO_2 polymorphs in fine sand") because genesis by inheritance of the heavy minerals of the fine sand of the soils, and their subsequent use in chronosequences to study the provenance of materials and their degree of alteration, is not an indisputable paradigm. For example, Tejan-Kella, Fitzpatrick, and Chittleborough (1991) found rutile and zircon grains with different degrees of alteration in the same profile, implying a complex environmental history (different provenances) in soils from a podzol chronosequence at Cooloola (Australia). Tejan-Kella et al. (1991), in Psamments and Orthods from South Australia, developed in sandy sediments of various ages, only found a weak tendency towards alteration over time in the heavy minerals. Farragallah and Essa (2011) found that the contents of relatively highly resistant minerals (sphene, rutile, garnet and zircon) followed an irregular distribution in both depth and time sequence in soils from different terraces of the River Nile near Assiut (Egypt). Sulieman et al. (2015) did not detect an increase in ultrastable heavy minerals (zircon, tourmaline and rutile) with increasing age of Nile terraces. In the present study, rutile or zircon were found in all profiles (Table S1).

The mineralogy of the heavy fine sand (Table S1, Figure S1) also reveals the decarbonatization undergone by the pre-Holocene profiles, because, unlike the Holocene soils and fresh point bar sediments of the Guadalquivir river course, they lack carbonate materials. In addition, the notable presence of anatase and rutile in the pre-Holocene soils is shown by the more intense reflections in the XRD diagrams (Figure S1). The high crystallinity, in some cases, of the rutile and anatase reflections could indicate that they are authigenic soil phases (see section "VP-SEM–EDX-Raman study of TiO_2 polymorphs in fine sand").

The VP-SEM–EDX analysis of the whole fine sand permitted observation of the sub-rounded shape of some grains, with somewhat polished surfaces, mechanical marking and a degree of sedimentological maturity (Figure 2c–f, i,j), in accordance with the fluvial origin of the parent material. Superficial features of chemical alteration were also observed in grains of various mineral species (Figure 2b,h–k). Quartz showed alteration features, even in the fine sands of the less developed soils, such as P5 (Figure 2b), in agreement with our previous results (Martín-García et al., 2004, 2015), which reported alteration features in quartz under a Mediterranean climate, even in scarcely evolved soils. Alteration was also observed in the grains of K-mica (Figure 2h), dolomite (Figure 2i), titanium oxides (Figure 2j) and titanite (Figure 2k), from both pre-Holocene (P1, P3) and Holocene soils (P4, P5). These observations give rise to the hypothesis that the alteration features are not necessarily produced in the same soil as that where the grain is currently found, and may be (particularly in less evolved, that is, Holocene, soils) inherited from fluvial sediments or from soils before those giving rise to the sediment. This would, therefore, involve the discussion of aspects such as polycyclism, superimposed features and diverse origins, previously described in zircon by Tejan-Kella et al. (1991), who stated that "the juxtaposition of euhedral, subeuhedral and unetched zircon and rutile grains with highly rounded and etched forms in the same profile indicates diverse provenance". This genetic complexity would thus imply that the VP-SEM–EDX observations of any grain do not provide sufficiently robust information on the effects of the age of the terraces, where the soils are found, on the fine sand grains. This has resulted in further investigation into the problem of the alteration of our fine sands using complimentary geochemical methods (ICPms). Another interesting observation with VP-SEM–EDX was the relatively greater presence of zircon grains in P1, the soil from the oldest terrace (600 ka, Table 1).

4.2 | TiO_2 polimorphs

The VP-SEM–EDX-Raman study of TiO_2 polimorphs in fine sand (Figure 3) implies that pedogenic neoformation of rutile has taken place in the study soils. However, the possibility that some grains of this mineral species, present in our fine sands, may be inherited cannot be ruled out. In no case did the rutile grains show any sign of alteration. Anatase was present in fine sand-sized grains, with some signs of weathering (Figure 3e,f), suggesting possible inheritance from the parent material.

The coexistence of the two polymorphs of TiO_2 rutile (neoformed/inherited) and anatase (inherited), shown by VP-SEM–EDX-Raman, is an original finding, particularly in Mediterranean fluvial terrace soils. Fitzpatrick and Chittleborough (2002) reported that evidence from both laboratory synthesis and field studies indicated that rutile should not necessarily be attributed to high-temperature formation and could also crystallize from an intermediate anatase phase. Rutile neoformation in soils has been assumed by Sun, Zhou, Du, and Xie (2017), whereas Cornu et al. (1999) showed, in tropical soils, the mobility of Ti and the neoformation of anatase, but never of rutile.

4.3 | Chemical composition

The SiO_2 content (Table S2) was positively correlated with that of quartz (Table S1) ($R^2 = 0.851$; $n = 24$). The

CaO content decreased dramatically in the pre-Holocene soils due to decarbonation and was positively correlated with calcite + dolomite (carbonates) ($R^2 = 0.887$; $n = 24$), and calcite ($R^2 = 0.854$; $n = 24$); MgO was correlated with dolomite ($R^2 = 0.775$; $n = 24$), as well as CaO and MgO ($R^2 = 0.762$; $n = 24$). A horizon of interest is 2Bwk2 of P4, with the "k" showing carbonate accumulation, which has very low percentages of CaO and MgO compared to the other horizons of the profile; the carbonates are found in the silt and clay fraction, as shown by the data of Calero (2005). As in the case of SiO_2, the amount of CaO in the fine sands in our soils contains valuable pedogenic information.

Major elements confirm the lithological discontinuity in 2Bwk2 (P4), shown by the XRD mineralogy (Table S1), with visibly higher values of SiO_2, Al_2O_3, Na_2O and K_2O, and lower values of CaO, Fe_2O_3 and MgO. In contrast, the lithological discontinuities of P5 were not accompanied by any notable change in chemical element composition.

The concentrations (means per profile) of some minor chemical elements, such as Mn, Sr, Cs, Hf and W (Table S3), showed dependence on the age groups of the soils (pre-Holocene vs. Holocene): Cs, Hf and W were more abundant in pre-Holocene soils; Mn and Sr were more abundant in Holocene soils. The maximum value of Zr (mean per profile) was that of P1.

The Ba and Zr content can be related to the presence of barite —$BaSO_4$— and zircon —$ZrSiO_4$—, respectively (Figure 2d,e,g), as can the content of ΣREE to that of monazite —(Ce,La,Nd,Pr)PO_4— (Figure 2h). The Mn content is related to the presence of ilmenite and andradite (garnet) because, although Mn does not belong to the ideal mineral formulae, it was detected in the VP-SEM–EDX spectra (Figure 2a,e,l). Furthermore, the positive correlations between Mn and Fe_2O_3 ($R^2 = 0.777$; $n = 24$) and TiO_2 ($R^2 = 0.726$; $n = 24$) suggest that, together with ilmenite and andradite, Mn may be linked to other Fe- and Ti-bearing minerals detected, such as biotite, goethite or haematite.

The Rb content positively correlates with total feldspars (K-feldspar + plagioclases; Table S1) ($R^2 = 0.717$; $n = 24$) and consequently shows high relative values (>105 mg kg^{-1}) in the P3 horizons, with maximum values of these minerals (23–38% K-feldspar + plagioclase; Table S1). The Rb content also positively correlates with K_2O ($R^2 = 0.908$; $n = 24$). Hossain et al. (2014) showed that Rb isomorphically substitutes for K in feldspars, which would explain our findings. However, Donaire (1995) explained that the significant positive correlation between Rb and K_2O in granitic rocks of the Los Pedroches Batholith (the zone of the present study) is due to the substitution of Rb by K in the K-mica, as also reported by Feng and Kerrich (1990) and Varga,

TABLE 2 Mean values of main geochemical indices for whole fine sand and clay fractions (weighted to horizon thickness). Standard deviation (*SD*) in parentheses

	SiO_2/CaO	CIW[a]	WIP[b]	WI[c]	BDI[d]	WR[e]	Sr/Zr[f]
Fine sand							
P1	795.58 (402.00)	92.61 (1.98)	17.21 (2.16)	2.56 (0.39)	0.28 (0.03)	31.66 (11.25)	0.12 (0.07)
P2	631.86 (583.59)	73.83 (27.51)	26.11 (6.42)	5.96 (4.40)	0.87 (0.50)	147.25 (178.85)	0.31 (0.11)
P3	206.26 (41.10)	79.76 (0.98)	38.15 (4.37)	4.95 (0.50)	0.60 (0.04)	97.76 (19.26)	0.41 (0.05)
P4	36.70 (50.35)	38.59 (24.60)	56.27 (17.01)	19.42 (10.52)	2.20 (1.14)	895.54 (563.11)	0.87 (0.50)
P5	2.53 (0.12)	17.08 (2.57)	78.02 (5.34)	30.49 (1.14)	3.81 (0.69)	1,287.03 (429.78)	2.21 (0.63)
PM	3.32	16.19	71.29	25.06	4.66	2,446.46	6.02
Clay							
P1		75.66 (6.79)	49.16 (3.67)		0.38 (0.10)	374.40 (52.26)	
P2		69.26 (4.53)	53.47 (2.38)		0.50 (0.08)	584.14 (92.30)	
P3		67.31 (9.63)	51.95 (4.53)		0.55 (0.18)	532.52 (87.50)	
P4		37.79 (17.26)	70.33 (9.42)		1.81 (1.01)	1,436.84 (561.84)	
P5		21.77 (7.03)	74.83 (5.19)		3.00 (1.11)	2,060.88 (179.62)	
PM		14.84	77.17		4.00	1,873.40	

[a]CIW, Chemical Index of Weathering (Harnois, 1988).
[b]WIP, Weathering Index of Parker (Parker, 1970).
[c]WI, Weathering Index (Vogel, 1975).
[d]BDI, Base Depletion Index (Jien et al., 2016).
[e]WR, Weathering Ratio (Chittleborough, 1991).
[f]Muhs et al. (2001).

Szakmány, Raucsik, and Máthé (2005). In our fine sands, Rb versus K-mica showed a positive correlation, albeit low ($R^2 = 0.167$; $n = 24$) and much lower than that of Rb versus total feldspars ($R^2 = 0.717$; $n = 24$), possibly due to the feldspars being more abundant than K-mica in most of our samples (Table S1).

The Sr content correlates with CaO ($R^2 = 0.863$; n = 24) and calcite ($R^2 = 0.815$; n = 24), which must be due to the well-known isomorphism between Sr and Ca. Cubillas, Hu, and Higgins (2015) suggested that Sr can be incorporated into the structure of natural and laboratory calcites (and may be a good indicator of the relative supersaturations of Sr vs. Ca at which the crystals grew).

The statistical relationship ($R^2 > 0.811$; $n = 24$) between pairs of elements within groups such as Mn-Ti-Fe, Cr-Ni-Mo, Sr-Ca, Rb-K and Hf-Th-U-REE, must be due to isomorphism (ion substitution in the crystal lattices). This process is regulated by Goldschmidt's rule (Misra, 2012), which postulates ionic substitutions when Δr is small (<15% of the radius of the smallest). The case of the group Mn^{3+}, Fe^{3+} and Ti^{4+} can be considered paradigmatic, because their radii (0.064, 0.064 and 0.068 nm, respectively) have Δr between 0 and 0.004 (never exceeding 7% of the smallest).

The chemical element composition (mean values per profile) of the whole fine sand (Tables S2 and S3) differed from that of the clay (Martín-García et al., 2019) in that the former contained lower quantities of major elements Al, Ca, Fe and K, and also lower quantities of most of the minor elements. This may be related, first, to the lower contents of phyllosilicates and, especially, the (hydr) oxides goethite and haematite, in the fine sand, and, second, to the role of the clay fraction as a scavenger of heavy elements (Martín-García et al., 2016). However, the higher content of Zr in the fine sand (except in point bar sediments), possibly due to the presence of zircon minerals (Table S1; Figures S1, 2d,e), should be noted. This mineral species, highly resistant to weathering, would tend to become concentrated through inheritance in the fine sand grains rather than the clay.

4.4 | Geochemical indices

The SiO_2/CaO ratio of the whole fine sand (Table 2) showed mean values greater than 200 (up to 795) in the pre-Holocene soils (P1, P2 and P3) and lower than 37 in the Holocene soils (P4, P5 and point bar sediments), reflecting the effect of soil age on this geochemical index. The presence of these two populations of SiO_2/CaO can be attributed to the two pedogenic processes, which combine and intensify with age: the leaching of carbonates, reducing CaO content, and the relative accumulation of quartz (main source of SiO_2), a mineral with relatively high resistance to alteration. This explains the correlations "SiO_2/CaO" versus "calcite" ($R^2 = 0.775$, logarithmic) and "SiO_2/CaO" versus "quartz" ($R^2 = 0.777$, logarithmic).

The CIW and WIP values also depend on age, ranging from 16.20 (point bar sediments) to 92.58 (P1) for the former and 78.02 (P5) to 17.22 (P1) for the latter. These results are similar to those of Price and Velbel (2003), where the CIW grew in parallel with alteration, fresh material being considered as that with CIW ≤50 (point bar sediments <20) and with maximum alteration at a value of 100 (P1 ≈ 93). For the WIP, Price and Velbel considered fresh material to have a value >100 with maximum alteration at 0. In the present study, although none of the profiles reached these extreme values, they were within the range 100 to 0. Ajmone-Marsan, Bain, and Duthie (1988) studied the WIP in fine sand of a soil chronosequence from northwest Italy, where the youngest soil (aged between 10–50 ka) showed a WIP of 41.7, and the oldest (500–750 ka) between 16.5 and 18.4, which are similar WIP and age values to the samples of the present study. Garzanti and Resentini (2016), studying fluvial point bar sands of Taiwanese rivers, reported values of a CIW between 48 and 95 and WIP between 18 and 65, close to those of our fine sands.

The WI and BDI of our whole fine sand (Table 2) persistently showed values related to age. The WI decreased from P1 (2.56) to P5–point bar sediments (30.49–25.07, respectively); the BDI increased from P1 (0.28) to point bar sediments (4.66). The BDI was determined by Jien et al. (2016) in a soil chronosequence from Taiwan (Arenosol, Cambisol, Lixisol and Ferralsol), showing values in fine earth (<2 mm) from 0.25 (soils of 20 ka) to 0.05 (soils of 80 ka). This tendency of the BDI to decrease with age coincided with our results, albeit with very different ranges of values. For example, our P3, with an age of 70 ka (Table 1), was comparable to the oldest Taiwanese soils studied by Jien et al. (2016), and showed a BDI of 0.59, whereas that of the equivalent Taiwanese soils was around 0.05. We believe that these divergences are due, in addition to our studying fine sand, to the lower intensity of pedogenic processes in the Mediterranean environment of our fluvial terraces (mean annual temperature 18°C, total annual precipitation 650 mm; soil types Fluvisol, Calcisol and Luvisol) compared to that in the ferralitic soils with the tropical oceanic climate of Taiwan (mean annual temperature 23.5°C, total annual precipitation 2,500 mm; soil types Arenosol, Cambisol, Lixisol, Acrisol and Ferralsol).

The WR values (Table 2), from 28.9 (P1) to 2,447.45 (point bar sediments), were also related to soil age. This

wide range is due to both the relative abundance of Ca in the Holocene soils and point bar sediments and to the relative concentration of Zr in the pre-Holocene soils (particularly in P1) (Tables S2, S3). Consequently, the content of carbonates (calcite + dolomite), the main source of CaO, is positively correlated with the WR ($R^2 = 0.761$; $n = 24$). Our WR values are much higher than those of Chittleborough (1991), which were between 3 and 22, as they were estimated in fine sand of soils lacking calcium carbonates. In the present study, Sr/Zr showed similar tendencies to the other indices and, because Sr^{2+} is diadochic with Ca^{2+} and Zr^{4+} increases in pre-Holocene soils, Sr/Zr decreased with age, from point bar sediments (6.02) to P1 (0.12) (Table S3).

Values of the geochemical indices for whole fine sand were generally similar to those of clay (Table 2). However, there were some cases with pronounced differences, such as the WR, which showed lower values in the whole fine sand than in the corresponding clay. This may be due to the higher relative concentration of Zr in the whole fine sand. The trends in the values of the indices with soil age were similar in clay and whole fine sand.

4.5 | Provenance of the soil materials

4.5.1 | Mineralogical evidences

The most abundant mineral species in our fine sands (Table S1) (phyllosilicates (muscovite/illite, biotite, paragonite, chlorite and interstratified minerals), quartz, feldspars (K-feldspar and plagioclases), iron oxides (goethite and haematite) and carbonates (calcite and dolomite)) have been described in the rocks of the source area (Carracedo et al., 1997; Jiménez-Espinosa et al., 2016; Larrea et al., 1992, 1994, 1995, 1996; Martínez et al., 2008; Martínez-Ruiz, 1994; Ortega-Huertas et al., 1991; Pascual et al., 2008; Pin et al., 2002; Torres-Ruiz et al., 2003). This suggests a potential provenance of the rocks/sediments through the process known as inheritance (Martín-García et al., 1998). However, the idea of provenance through inheritance requires further explanation in some cases. For example, calcite may also originate from neoformation in those horizons where it accumulates pedogenically (e.g., Cmk/Bt of P2). Goethite and haematite may be both neoformed and inherited. The process of transformation may be partly responsible, for example, for the presence of interstratified minerals (Calero et al., 2013).

Because the mineral contents change over time due to soil evolution, the idea of provenance of soil materials (by comparison between soil materials and rocks of the source area) is only applicable to young soils and point bar sediments. The minor minerals are often used as indicators of provenance (von Eynatten & Dunkl, 2012). In the present study, most of the mineral species detected (Table S1, Figures 2 and 3) have also been cited as rock-forming minerals of the source area (river basin) materials of the fluvial terraces, and would be inherited from them in our fine sands (see section "Minor elements" in "Chemical composition"). However, some of these minor phases require further discussion because the type of rock from which they originate is clear. For example, garnet, staurolite and andalusite are of metamorphic origin in the Iberian Massif (Larrea et al., 1992, 1994, 1995, 1996) and the Internal Betic Zone (Torres-Ruiz et al., 2003). The variety of garnet found in P2 (horizons Btg1 and Btg2) and P4 (4C2) (Figure 2a) is andradite, typical of contact metamorphosed rocks when the wallrock is limestone (Klein & Dutrow, 2007), which is perfectly feasible in zones close to the Los Pedroches Batholith (Tornos & Chiaradia, 2004). The staurolite (Figure 2j) found in P4 (horizon 4C2) is a medium to high-grade metasedimentary mineral (regional metamorphism) and, in the source area, has been described in the metapelites of the Internal Zone of the Betic Cordillera (Díaz de Federico, Puga, Burgos, Gallegos, & Sanz de Galdeano, 1980). Rutile could also be employed as an indicator of provenance as it is present in most of the rocks of this zone. However, evidence that it may be neoformed (section "VP-SEM–EDX-Raman study of TiO_2 polymorphs in fine sand") tends to invalidate this possibility.

4.5.2 | Geochemical evidence

The spider diagrams of the chondrite-normalized chemical composition of selected elements in the whole fine sand (Figure S2), again show (sections "Chemical composition" and Tables S2 and S3) that, due to the effect of time, composition differs between soils. Furthermore, its relationship with all the geological materials of the zone, potential providers of materials, is clear. However, the closest relationships (in all elements, from Fe to Ba) are with the sedimentary rocks (Martínez-Ruiz, 1994; Ortega-Huertas et al., 1991) (Figure S2b). Figure S2 also shows the expected geochemical relationship between the whole fine sand and the clay (Martín-García et al., 2016), although clay contained more Fe and V, and the former more Zr (except in point bar sediments).

The geochemical indices were used as fingerprints of provenance (Garzanti & Resentini, 2016) by comparing the values of the samples with those of the geological materials (Figure 4). According to the CIW (Figure 4a), the fine sands and clays of the pre-Holocene soils (P1, P2 and P3) would be related (similar range of values) to the

TABLE 3 Chronofunctions of mineralogical and chemical variables and geochemical indices (y) measured in the whole fine sand and clay (only geochemical indices) of soil horizons and averaged[a] ($n = 6$, $p < .05$), x = ka

	Linear		Logarithmic		Quadratic	
	Equation	**r**	**Equation**	**r**	**Equation**	**r**
Whole fine sand						
1.23–1.53 nm phases XRD/%	$y = 0.011x + 1.179$	0.853			$y = 4E{-}05x^2{-}0.012x + 1.864$	0.974
Quartz XRD/%			$y = 2.936\ln(x) + 41.083$	0.837		
Goethite XRD/%					$y = 2E{-}05x^2{-}0.008x + 1.812$	0.968
Calcite XRD/%			$y = -2.561\ln(x) + 17.940$	−0.930		
CaO/%			$y = -1.676\ln(x) + 12.016$	−0.887		
P_2O_5/%			$y = -0.007\ln(x) + 0.0737$	−0.863		
Cr/mg kg^{-1}					$y = -0.001x^2 + 0.889x + 8.568$	−0.897
Ni/mg kg^{-1}					$y = -0.001x^2 + 0.412x + 3.844$	−0.897
Sr/mg kg^{-1}			$y = -30\ln(x) + 212.460$	−0.964		
Zr/mg kg^{-1}			$y = 9.897\ln(x) + 146.220$	0.852		
Mo/mg kg^{-1}					$y = -3E{-}05x^2 + 0.022x$ - 0.038	−0.909
Hf/mg kg^{-1}	$y = 0.003x + 1.031$	0.907	$y = 0.136\ln(x) + 1.312$	0.815	$y = 2E{-}06x^2 + 0.002x + 1.073$	0.912
W/mg kg^{-1}	$y = 0.004x + 0.848$	0.840			$y = -2E{-}05x^2 + 0.013x + 0.563$	−0.982
U/mg kg^{-1}	$y = 0.002x + 1.0812$	0.850			$y = 5E{-}06x^2{-}0.001x + 1.161$	0.919
ΣREE/mg kg^{-1}	$y = 0.107x + 68.157$	0.873			$y = 2E{-}04x^2{-}0.008x + 71.653$	0.905
SiO_2/CaO	$y = 1.381x + 54.367$	0.964			$y = -0.0026x^2 + 2.869x + 9.189$	0.9998
CIW			$y = 5.939\ln(x) + 42.930$	0.897		
WIP	$y = -0.086x + 61.89$	−0.851	$y = -4.268\ln(x) + 55.088$	−0.874	$y = 2E{-}04x^2{-}0.227x + 66.152$	0.923
WI			$y = -1.972\ln(x) + 18.086$	−0.842		
BDI			$y = -0.348\ln(x) + 2.661$	−0.965		
WR			$y = -185.4\ln(x) + 1{,}132.2$	−0.989		
Sr/Zr			$y = -0.434\ln(x) + 2.393$	−0.965		
Clay						
CIW			$y = 4.902\ln(x) + 39.453$	0.937		
WIP			$y = -2.248\ln(x) + 66.633$	−0.897		
BDI			$y = -0.295\ln(x) + 2.207$	−0.980		
WR			$y = -128.4\ln(x) + 1{,}361.0$	−0.873		

[a]Mean profile values (from Tables 2, S1, S2 and S3) weighted to horizon thickness.

Abbreviations: BDI, Base Depletion Index; CIW, Chemical Index of Weathering; WIP, Weathering Index of Parker; WI, Weathering Index; WR, Weathering Ratio.

igneous and metasedimentary rocks, whereas the fine sands and clays of the Holocene soils (P4 and P5) and point bar sediments would be related to the sedimentary rocks. According to the WIP (Figure 4a), the Holocene soils are in the middle of the range of all the rocks from the source area and the pre-Holocene soils would separate from them. The values of the BDI (Figure 4b) reiterate the behaviour of the CIW. This once again demonstrates that the values of these indices for our samples depend on age and that the indices are not decisive for determining provenance. However, the information obtained from Figure 4a,b overcame the simple use of geochemical indices as a provenance tool: first, through the possible predictive value between indices on showing that there are correlations with a high coefficient of determination between the CIW versus the WIP (negative) and the WIP versus the BDI (positive), for both the fine sand and clay fractions; and second, because they

reveal that the lines of the two granulometric fractions intersect at a critical point (geometrical point common to both), after which they diverge (Figure 4a,b). This permits formulation of the hypothesis that the critical point is related to "time zero" for granulometric evolution; that is, when there is no size differentiation. It also supports the hypothesis that the critical point indicates "time zero" for pedogenic evolution. Both hypotheses are confirmed by Figure 4a,b, which shows the critical point close to the least evolved materials studied: point bar sediments and Holocene soil P5. New evidence to support these hypotheses is the great similarity between the defining coordinates (values) of the critical point (CP): $CP_{WIP\ (versus\ CIW)} = 80.76$, very close to $CP_{WIP\ (versus\ BDI)} = 79.39$. This value (≈80) is close to 100, the value of the WIP for fresh material given by Price and Velbel (2003). The value of $CP_{CIW\ (versus\ WIP)}$ is 15.46, ≤50, attributed to the unaltered samples by Price and Velbel.

4.6 | Soil fine sand chronofunctions

In order to better quantify the relationships of the different properties of the whole fine sand with age, chronofunctions were calculated (Table 3). Most were logarithmic ($y = a{\cdot}lnx + b$) and quadratic ($y = ax^2 + bx + c$) and, to a lesser extent, linear ($y = ax + b$); this can be interpreted as indicating that these parameters will reach their steady state (Schaeltz, Barrett, & Winkler, 1994) and prove the existence of an authentic soil chronosequence, previously demonstrated by other compositional and morphological properties of the soils of the chronosequence (Calero et al., 2008, 2009, 2013; Martín-García et al., 2016, 2019). No previous studies of chronofunctions established using soil fine sand have been found in the bibliography.

The equations obtained also provided other information. The curves, which decreased with the age of calcite, CaO and Sr (CaO and Sr associated with the carbonates), quantify the process, detected previously, of loss of carbonates through dissolution/alteration over time. This is 0.057% every 1,000 years for calcite. The opposite (curve increases with age) occurs in quartz, which accumulates through inheritance in the soil fine sand over time, at a rate of 0.065% every 1,000 years, similar to the rate of calcite loss.

The Zr chronofunction also increases, in this case due to the Zr-bearing mineral zircon, which remains in the fine sand fraction (Figure 2d,e). The same also occurs in Hf, U and REE, which, as elements with low mobility, may be associated with the mineral monazite (Figure 2b, h). The positive chronofunction of the 1.23–1.53 nm phases, indicates the transformation of 2:1 phases, increasing with age, and which was demonstrated using chronofunctions of the nanoparameters of the clay fraction of our soils by Calero et al. (2013).

The geochemical alteration indices SiO_2/CaO, CIW, WIP, WI, BDI, WR and Sr/Zr mainly exhibited logarithmic fitting in their chronofunction (Table 3), suggesting not only dependence on age but also that the alteration of the fine sands will attain steady state. The chronofunction BDI = −0.348 ln(age in ka) + 2.659 (Table 3) implies that, for an age of 600 ka (maximum investigated; Table 1) the BDI of the fine sand is 0.43. When this value is interpolated in the chronofunction for fine earth of Taiwanese soils reported by Jien et al. (2016), BDI = 1/(1 + 0.21 × age in ka), the age required to attain this BDI is 6.2 ka. The great difference between 600 and 6.2 ka (~100 lower) is due to the Mediterranean climate of our chronosequence being much less pedogenically active than the tropical climate of Taiwan (section "Geochemical indices"). Thus, environmental conditions (soil-forming factors) and soil classification must be considered when interpreting alteration indices in soil chronosequences.

The chronofunction equations obtained for the alteration indices (Table 3) also permit further discussion regarding the critical point (Figure 4) and the hypothesis that it represents "time zero" for soil formation or the start of alteration. When the equations are extrapolated to zero (or close to zero) for 0.001 ka (age attributed to point bar sediments; Table 1) the WIP has a value (logarithmic) of 84.56, not only close to 71.34, the WIP value calculated for point bar sediments with the analytical data (Table 2), but also very close to those of CP_{WIP}, established in a completely different manner in Figure 4a,b: 80.76 and 79.39. This confirms an initial WIP of 70–80 in our soils and that critical point represents "time zero." Furthermore, the BDI values were extrapolated$_{(0.001\ ka)} = 5.06$, calculated in point bar sediments = 4.66, and $CP_{BDI} = 4.11$, which, due to their relative similarity, confirm an initial BDI value (without alteration) of between 4 and 5 and, once again, that CP represents "time zero."

5 | CONCLUSION

Fine sands are suggested as a granulometric fraction of great pedogenic interest, with the advantage of their easiness of extraction and analysis. Our results demonstrate the usefulness of fine sand in discussing the origin of the different minerals it contains, pedogenic alteration and the provenance of soil materials, even being able to establish chronosequences between properties of fine sand and soil age. Furthermore, pedogenetic rutile neoformation, never previously described, was reported,

as was its coexistence with its polymorph, anatase. Finally, we think that our results may be useful in sedimentology, because these soils are a potential source of sediment.

ACKNOWLEDGEMENTS

Sample preparation and chemical analysis (ICPms and ICP-AES) were conducted by Emma Humphreys-Williams and Stanislav Strekopytov (Imaging and Analysis Centre, Natural History Museum, London). VP-SEM images and EDX and Raman analysis were conducted by Isabel Guerra (Centro de Instrumentación Científica, Universidad de Granada, Spain). We thank Professor Dr Gabriel Delgado for his invaluable advice on the analytical techniques to employ in this study. This work was supported by a grant from Ministerio de Economía, Industria y Competitividad de España ("Mediterranean Soil Typologies versus Quartz. At the frontier of pedogenic knowledge"; Ref. CGL2016-80308-P). We thank Robert Abrahams (BSc) for revising the English language.

CONFLICT OF INTEREST

None.

AUTHOR CONTRIBUTIONS

JMM-G, JC and RD sampled the soils and separated the fine sand fraction and heavy fine sand fraction. JMM-G, JC, MS-M and RD carried out the XRD study. The ICPms was carried out at the Natural History Museum of London, and the results were interpreted by JMM-G, AM-G and RD. The VP-SEM and Raman study was carried out by JMM-G, AM-G, MVF-G and RD. All the authors wrote the manuscript.

DATA AVAILABILITY STATEMENT

The data are available on request from the authors

ORCID

Juan M. Martín-García https://orcid.org/0000-0003-0759-0640

Alberto Molinero-García https://orcid.org/0000-0003-0213-4814

Julio Calero https://orcid.org/0000-0003-2606-307X

REFERENCES

Ajmone-Marsan, F., Bain, D. C., & Duthie, D. M. L. (1988). Parent material uniformity and degree of weathering in a soil chronosequence, northwestern Italy. *Catena*, *15*, 507–517.

Arnold, R. W. (1968). Pedological significance of lithologic discontinuities. In J.W. Holmes. (Ed.), *Transactions, 9th International Congress of Soil Science* (Vol. 4, pp. 595–603). Adelaide, Australia: The International Society of Soil Science and Angus and Robertson LTD.

Arsov, L. D., Kormann, C., & Plieth, W. (1991). Electrochemical synthesis and in situ Raman spectroscopy of thin films of titanium dioxide. *Journal of Raman Spectroscopy*, *22*, 573–575.

Calero, J. (2005). *Génesis de la fracción mineral y de la ultramicrofábrica en una cronosecuencia de suelos sobre terrazas del río Guadalquivir* (Doctoral dissertation). Universidad de Granada, Granada.

Calero, J., Delgado, R., Delgado, G., & Martín-García, J. M. (2008). Transformation of categorical field soil morphological properties into numerical properties for the study of chronosequences. *Geoderma*, *145*, 278–287.

Calero, J., Delgado, R., Delgado, G., & Martín-García, J. M. (2009). SEM image analysis in the study of a soil chronosequence on fluvial terraces of the middle Guadalquivir (southern Spain). *European Journal of Soil Science*, *60*, 465–480.

Calero, J., Martín–García, J. M., Delgado, G., Aranda, V., & Delgado, R. (2013). A nano-scale study in a soil chronosequence from southern Spain. *European Journal of Soil Science*, *64*, 192–209.

Carracedo, M., Larrea, F. J., Alonso-Olazabal, A., & Gil-Ibarguchi, J. I. (1997). The relationship between the plutonic intrusions and the dyke swarm in the Los Pedroches batholith (Iberian Massif, Spain): Dykes as a paleotectonic and paleostress indicators. *Cadernos del Laboratorio Xeolóxico de Laxe*, *22*, 229–246.

Carral, M. P., Martín-Serrano, A., Sansteban, J. I., Guerra, A., & Jiménez-Ballesta, R. (1998). Los factores determinantes en la secuencia edáfica de la evolución morfodinámica del tramo medio del Guadalquivir (Jaén). *Revista de la Sociedad Geológica de España*, *11*, 111–126.

Chittleborough, D. J. (1991). Indices of weathering in soils and palaeosols formed on silicate rocks. *Australian Journal of Earth Sciences*, *38*, 115–120.

Cornu, S., Lucas, Y., Lebon, E., Ambrosi, J. P., Luizao, F., Rouiller, J., … Neal, C. (1999). Evidence of titanium mobility in soil profiles, Manaus, central Amazonia. *Geoderma*, *91*, 281–295.

Cubillas, P., Hu, X., & Higgins, S. R. (2015). Strontium incorporation during calcite growth: Implications for chemical mapping using friction force microscopy. *Chemical Geology*, *411*, 274–282.

Delgado, R., Martín-García, J. M., Oyonarte, C., & Delgado, G. (2003). Genesis of the *terrae rossae* of the Sierra Gádor (Andalusia, Spain). *European Journal of Soil Science*, *54*, 1–16.

Díaz de Federico, A., Puga, E., Burgos, J., Gallegos, J. A., & Sanz de Galdeano, C. (1980). *Mapa geológico de España a escala 1: 50.000 (hoja 1027)*. Madrid, Spain: Instituto Geológico y Minero de España (IGME).

Donaire, T. (1995). *Petrología y geoquímica de las rocas granitoides y enclaves asociados del batolito de Los Pedroches (Macizo Ibérico)* (Doctoral dissertation). Universidad de Huelva, Huelva, Spain.

Farragallah, M. A., & Essa, M. A. (2011). Sand and clay mineralogical composition in relation to origin, sedimentation regime, uniformity, and weathering rate of Nile terrace soils at Assiut, Egypt. *Australian Journal of Basic and Applied Sciences*, *5*, 239–256.

Feng, R., & Kerrich, R. (1990). Geochemistry of fine-grained clastic sediments in the Archean Abitibi greenstone belt, Canada: Implications for provenance and tectonic setting. *Geochimica et Cosmochimica Acta*, *54*, 1061–1081.

Fitzpatrick, R. W., & Chittleborough, D. J. (2002). Titanium and zirconium minerals. In J. B. Dixon & D. G. Schulze (Eds.), *Soil mineralogy with environmental applications. Soil Science Society of America Book Series No. 7* (pp. 667–690). Madison, WI: Soil Science Society of America Inc.

Garzanti, E., & Resentini, A. (2016). Provenance control on chemical indices of weathering (Taiwan river sands). *Sedimentary Geology*, *336*, 81–95.

Harnois, L. (1988). The CIW index: A new chemical index of weathering. *Sedimentary Geology*, *55*, 319–322.

Hernández-Hinojosa, V., Montiel-García, P. C., Armstrong-Altrin, J. S., Nagarajan, R., & Kasper-Zubillaga, J. J. (2018). Textural and geochemical characteristics of beach sands along the western Gulf of Mexico, Mexico. *Carpathian Journal of Earth and Environmental Sciences*, *13*, 161–174.

Hossain, I., Roy, K. K., Biswas, P. K., Alam, M., Moniruzzaman, M., & Deeba, F. (2014). Geochemical characteristics of Holocene sediments from Chuadanga district, Bangladesh: Implications for weathering, climate, redox conditions, provenance and tectonic setting. *Chinese Journal of Geochemistry*, *33*, 336–350.

Jien, S. H., Baillie, I., Huang, W. S., Chen, Y. Y., & Chiu, C. Y. (2016). Incipient ferralization and weathering indices along a soil chronosequence in Taiwan. *European Journal of Soil Science*, *67*, 583–596.

Jiménez-Espinosa, R., Jiménez-Millán, J., & García-Tortosa, F. J. (2016). Upper-Pleistocene terrace deposits in Mediterranean climate: Geomorphological and source-rock control on mineral and geochemical signatures (Betic Cordillera, SE Spain). *Journal of Iberian Geology*, *42*, 187–200.

Klein, C., & Dutrow, B. (2007). *Mineral science*. New York, NY: Wiley.

Larrea, F. J., Carracedo, M., Cueto, L. A., Quesada, C., Gil-Ibarguchi, J. I., Fernández, F. J., & Ortega, L. A. (1992). Petrology and geochemistry of Cardeña-Virgen de La Cabeza pluton (batholith of Los Pedroches). *Cuadernos do Laboratorio Xeolóxico de Laxe*, *17*, 209–222.

Larrea, F. J., Carracedo, M., Ortega, L. A., & Gil-Ibarguchi, J. I. (1994). The Linares granite (Jaén): Cartography, petrology and geochemistry. *Cadernos do Laboratorio Xeolóxico de Laxe*, *19*, 335–346.

Larrea, F. J., Carracedo, M., Ortega, L. A., & Gil-Ibarguchi, J. I. (1995). The Santa Elena stock (Jaén). An intrusion genetically independent from the magmatic association of the Los Pedroches Batolith. *Cadernos do Laboratorio Xeolóxico de Laxe*, *20*, 151–166.

Larrea, F. J., Carracedo, M., Yusta, I., Ortega, L. A., & Gil-Ibarguchi, J. I. (1996). Los diques traquiandesíticos asociados al plutón granodiorítico de Los Pedroches (batolito de Los Pedroches, España). *Geogaceta*, *20*, 586–589.

Liu, B., Jin, H., Sun, Z., & Zhao, S. (2016). Geochemical weathering of aeolian sand and its palaeoclimatic implications in the Mu Us Desert, northern China, since the Late Holocene. *Journal of Arid Land*, *8*, 647–659.

McDonough, W. F., & Sun, S. (1995). The composition of the Earth. *Chemical Geology*, *120*, 223–253.

Martínez, J., Llamas-Borrajo, J., de Miguel-García, E., Rey-Arrans, J., Hidalgo-Estévez, M. C., & Sáez-Castillo, A. J. (2008). Multivariate analysis of contamination in the mining district of Linares (Jaén, Spain). *Applied Geochemistry*, *23*, 2324–2336.

Martínez-Ruiz, F. (1994). *Geoquímica y mineralogía del tránsito Cretácico-Terciario en las Cordilleras Béticas y en la Cuenca Vasco-Cantábrica* (Doctoral dissertation). Universidad de Granada, Granada.

Martín-García, J. M., Aranda, V., Gámiz, E., Bech, J., & Delgado, R. (2004). Are Mediterranean mountains Entisols weakly developed? The case of Orthents from Sierra Nevada (Southern Spain). *Geoderma*, *118*, 115–131.

Martín-García, J. M., Delgado, G., Párraga, J. F., Bech, J., & Delgado, R. (1998). Mineral formation in micaceous Mediterranean Red soils of Sierra Nevada, Granada, Spain. *European Journal of Soil Science*, *49*, 253–268.

Martín-García, J. M., Delgado, G., Sánchez-Marañón, M., Párraga, J. F., & Delgado, R. (1997). Nature of dioctahedral micas in Spanish red soils. *Clay Minerals*, *32*, 107–121.

Martín-García, J. M., Márquez, R., Delgado, G., Sánchez-Marañón, M., & Delgado, R. (2015). Relationships between quartz weathering and soil type (Entisol, Inceptisol and Alfisol) in Sierra Nevada (southeast Spain). *European Journal of Soil Science*, *66*, 179–193.

Martín-García, J. M., Molinero-García, A., Calero, J., Fernández-González, M. V., Párraga, J., & Delgado, R. (2019). Lanthanides in granulometric fractions of Mediterranean soils. Can they be used as fingerprints of provenance? *European Journal of Soil Science*, *70*, 394–410.

Martín-García, J. M., Sánchez-Marañón, M., Calero, J., Aranda, V., Delgado, G., & Delgado, R. (2016). Iron oxides and rare earth elements in the clay fractions of a soil chronosequence in southern Spain. *European Journal of Soil Science*, *67*, 749–762.

Misra, K. C. (2012). *Introduction to geochemistry. Principles and applications*. Oxford, England: Wiley-Blackwell.

Muhs, D. R., Bettis, E. A., Been, J., & McGeehin, J. P. (2001). Impact of climate and parent material on chemical weathering in loess-derived soils of the Mississippi river valley. *Soil Science Society of America Journal*, *65*, 1761–1777.

Ortega-Huertas, M., Palomo, I., Moresi, M., & Oddone, M. (1991). A mineralogical and geochemical approach to establishing a sedimentary model in a passive continental margin (Subbetic zone, Betic Cordilleras, SE Spain). *Clay Minerals*, *26*, 389–407.

Parker, A. (1970). An index of weathering for silicate rocks. *Geological Magazine*, *107*, 501–504.

Pascual, E., Donaire, T., & Pin, C. (2008). The significance of microgranular enclaves in assessing the magmatic evolution of a high-level composite batholith: A case on the Los Pedroches Batholith, Iberian Massif, Spain. *Geochemical Journal*, *42*, 177–198.

Pin, C., Liñán, E., Pascual, E., Donaire, T., & Valenzuela, A. (2002). Late Neoproterozoic crustal growth in the European Variscides: Nd isotope and geochemical evidence from the Sierra de Córdoba Andesites (Ossa-Morena Zone, Southern Spain). *Tectonophysics*, *352*, 133–151.

Price, J. R., & Velbel, M. A. (2003). Chemical weathering indices applied to weathering profiles developed on heterogeneous felsic metamorphic parent rocks. *Chemical Geology*, *202*, 397–416.

Santos-García, J.A. (1988). *Informe sedimentológico sobre las terrazas del río Guadalquivir*. Estudio geológico-hidrogeológico de la zona de Andujar (Jaén). Tomo IV-I: Estudio hidrogeológico de detalle 1:10000. Technical report. Madrid, Spain: ENRESA. pp. 56–72.

Santos-García, J. A., Jerez-Mir, F., & Saint-Aubin, J. (1991). Estudio sedimentológico de un sector del río Guadalquivir en las proximidades de Andújar (provincia de Jaén). Los depósitos de la terraza +6m (T4). *Estudios Geológicos*, *47*, 43–55.

Schaeltz, R. J., Barrett, L. R., & Winkler, J. A. (1994). Choosing models for soil chronofunctions and fitting them to data. *European Journal of Soil Science*, *45*, 219–232.

Schaetzl, R. J., & Thompson, M. L. (2015). *Soil genesis and geomorphology*. New York, NY: Cambridge University Press.

Sulieman, M. M., Ibrahim, I. S., Elfaki, J. T., & Dafa-Allah, M. S. (2015). Origin and distribution of heavy minerals in the surficial and subsurficial sediments of the alluvial Nile River terraces. *Open Journal of Soil Science*, *5*, 299–310.

Sun, Z., Zhou, D., Du, J., & Xie, Y. (2017). Low temperature self-assembled growth of rutile TiO_2/manganese oxide nanocrystalline films. *Applied Surface Science*, *420*, 489–495.

Tamm, O. (1937). Om de lagproduktiva sandmarkerna a Hökensas och i övre Lagadalen. *Meddelanden från Statens skogsförsöksanstalt*, *30*, 1–66.

Tejan-Kella, M. S., Chittleborough, D. J., & Fitzpatrick, R. W. (1991). Weathering assessment of heavy minerals in age sequences of Australian sandy soils. *Soil Science Society of America Journal*, *55*, 427–434.

Tejan-Kella, M. S., Fitzpatrick, R. W., & Chittleborough, D. J. (1991). Scanning electron microscope study of zircons and rutiles from a podzol chronosequence at Cooloola, Queensland, Australia. *Catena*, *18*, 11–30.

Tornos, F., & Chiaradia, M. (2004). Plumbotectonic evolution of the Ossa Morena zone, Iberian Peninsula: Tracing the influence of mantle-crust interaction in ore-forming processes. *Economic Geology*, *99*, 965–985.

Torres-Ruiz, J., Pesquera, A., Gil-Crespo, P. P., & Velilla, N. (2003). Origin and petrogenetic implication of turmaline-rich rocks in the Sierra Nevada (Betic Cordillera, southeastern Spain). *Chemical Geology*, *197*, 55–86.

Varga, A. R., Szakmány, G., Raucsik, B., & Máthé, Z. (2005). Chemical composition, provenance and early diagenetic processes of playa lake deposits from the Boda Siltstone Formation (Upper Permian), SW Hungary. *Acta Geologica Hungarica*, *48*, 49–68.

Vogel, D. E. (1975). Precambrian weathering in acid metavolcanic rocks from the Superior Province, Villebon Township, South-Central Quebec. *Canadian Journal of Earth Sciences*, *12*, 2080–2085.

von Eynatten, H., & Dunkl, I. (2012). Assessing the sediment factory: The role of single grain analysis. *Earth-Science Reviews*, *115*, 97–120.

SUPPORTING INFORMATION

Additional supporting information may be found online in the Supporting Information section at the end of this article.

How to cite this article: Martín-García JM, Molinero-García A, Calero J, Sánchez-Marañón M, Fernández-González MV, Delgado R. Pedogenic information from fine sand: A study in Mediterranean soils. *Eur J Soil Sci*. 2020;1–18. https://doi.org/10.1111/ejss.12935